

1 Article

2 Changes in CO₂ Adsorption Affinity Related to Ni Doping in 3 FeS Surfaces: A DFT-D3 Study

4 Aleksandar Živković^{1,*}, Michiel Somers¹, Eloi Camprubi¹, Helen E. King¹, Mariette Wolthers^{1,*} and Nora H. de
5 Leeuw^{1,2,3,*}

6 ¹ Department of Earth Sciences, Utrecht University, Princetonlaan 8a, 3584CB Utrecht, The Netherlands

7 ² School of Chemistry, University of Leeds, Leeds LS2 9JT, United Kingdom

8 ³ School of Chemistry, Cardiff University, Park Place, Cardiff CF10 3AT, United Kingdom

9 *Corresponding authors: A.Zivkovic@uu.nl, M.Wolthers@uu.nl, N.H.deLeeuw@uu.nl

10 **Abstract:** Metal sulphides constitute cheap, naturally abundant, and environmentally friendly
11 materials for energy storage applications and chemistry. In particular, iron (II) monosulphide (FeS,
12 mackinawite) is a material of relevance in theories of the origin of life and for heterogenous
13 catalytic applications in the conversion of carbon dioxide (CO₂) towards small organic molecules.
14 In natural mackinawite Fe is often substituted by other metals, however, little is known about how
15 such substitutions alter the chemical activity of the material. Herein, the effect of Ni doping on the
16 structural, electronic, and catalytic properties of FeS surfaces is explored via dispersion-corrected
17 density functional theory simulations. Substitutional Ni dopants, introduced on the Fe site, are
18 readily incorporated into the pristine matrix of FeS, in good agreement with experimental
19 measurements. The CO₂ molecule was found to undergo deactivation and partial desorption from
20 the doped surfaces, mainly at the Ni site when compared to undoped FeS surfaces. This behaviour
21 is attributed to the energetically lowered *d*-band centre position of the doped surface, as a
22 consequence of the increased number of paired electrons originating from the Ni dopant. The
23 reaction and activation energies of CO₂ dissociation atop the doped surfaces were found to be
24 increased when compared to pristine surfaces, thus helping to elucidate further the role Ni could
25 have played in the reactivity of FeS. It is expected that Ni-doping in other Fe-sulphides may have
26 a similar effect, limiting the catalytic activity of these phases when this dopant is present at their
27 surfaces.

28 **Keywords:** iron sulphides; mackinawite; density functional theory; carbon dioxide (CO₂)
29 adsorption; nickel doping

31 1. Introduction

32 The production of fuels and organic molecule feedstock from captured CO₂ and a
33 hydrogen source, e.g. water, using renewable energy sources is considered a promising
34 route towards achieving a sustainable and green future [1]. For example, renewable
35 sources often generate electrical energy that exceeds demand. This excess energy could
36 be used to transform captured CO₂ to chemicals and fuels, converting this electrical
37 energy to a store of chemical energy for future use [2–4]. In addition, the electrocatalytic
38 reduction of CO₂ represents a clean and efficient way to produce valuable fuels (such as
39 alcohols or hydrocarbons) or fuel precursors through CO₂ recycling [5,6]. A key
40 requirement for an effective conversion of CO₂ is the development of efficient and
41 inexpensive catalysts, which at the same time demonstrate sufficient durability, activity,
42 and selectivity towards valuable products [7].

43 Transition metal sulphides constitute a group of naturally generated materials with
44 arguably the most diverse electrical and magnetic properties available. They include
45 materials with a variety of properties, including diamagnetic insulators (ZnS),
46 diamagnetic semiconductors (PbS), antiferromagnetic semiconductors (CuFeS₂),
47 ferrimagnetic (Fe₇S₈) and antiferromagnetic metallic conductors (Fe₉S₁₀) or Pauli
48 paramagnetic metals ((Ni,Fe)₉S₈), just to name a few [8–10]. Amongst those, iron
49 sulphides constitute a distinct group of solids and complexes that play a key role in
50 marine systems and global biogeochemical sulphur cycles, which are central to
51 fundamental concepts about the evolution of the Earth surface environment [11]. More
52 importantly, they have been associated as catalysts in a number of key biochemical
53 reactions related to *Origin of Life* theories [11–17] and more recently, as a potential
54 electron source for autotrophic denitrification [18], as well as chromium [19] and
55 vanadium removal [20]. Due to the variety in composition and structure of iron
56 sulphides, a broad range of oxidation states is possible for both the iron and sulphur,
57 which consequently makes these minerals remarkably reactive [8,21].

58 In this work, the effect of nickel substitution for iron on the catalytic properties of
59 mackinawite (tetragonal FeS) towards CO₂ adsorption, activation and reduction is
60 assessed using calculations based on the density functional theory (DFT). Earlier studies
61 have elucidated the interaction of mackinawite surfaces with NO_x gases [22],
62 methylamine [23], carbon dioxide [24], arsenous acid [25], cysteine [26], water [27,28],
63 trichloroethylene [29], uranium [30], and mercury [31], amongst various other
64 adsorbates. However, considerably less information is available in the literature on the
65 adsorption properties of doped mackinawite. According to early studies conducted by
66 Morse *et al* [32], there is evidence that naturally formed FeS can accommodate significant
67 concentrations of metals other than Fe, e.g., Cu, Co, and Ni. Cody *et al* [16] noted that
68 natural metal sulphides rarely are compositionally pure, rather extensive cationic
69 substitutions are often encountered. Even a minor amount of substitution, e.g., Ni²⁺ for
70 Fe²⁺ in FeS or Mn²⁺ for Zn²⁺ in ZnS was postulated to induce significant changes in
71 catalytic properties, yet the effect has not been studied in detail [21]. Kwon *et al* [33] have
72 employed DFT calculations to examine the structural effects of both substitutional and
73 intercalated transition metals (namely Co, Ni, and Cu) incorporated into bulk FeS. The
74 authors found that metal incorporation into mackinawite most likely occurs via
75 substitution, which was further inferred to influence phase transformation pathways of
76 mackinawite.

77 Wilkin *et al* [34] examined the uptake of Ni by synthetic FeS mackinawite. Rapid
78 and efficient Ni uptake was observed for FeS, consistent with previous studies of Hg, Pb,
79 and Cd incorporation. Ikogou *et al* [35] observed Ni(II) successfully substituting Fe(II) in
80 the structure of biogenic mackinawite together with the possible influence of Ni on the
81 stabilization and delay of the transformation of mackinawite into pyrite (FeS₂). A similar
82 conclusion was reached by Swanner *et al* [36], who noted a kinetic inhibition to the
83 formation of pyrite in the presence of Co and Ni.

84 Despite the observations and expectations on the effects of Ni on the properties of
85 mackinawite, there is little specific information on how dopants may alter its catalytic
86 activity. The present study therefore aims to provide a detailed understanding of a Ni-
87 doped FeS system and its potential application as a catalytic material for CO₂
88 adsorption. Some of the -research questions of interest that this study aims to elucidate
89 are:

- 90 (1) What is the energetic cost to form Ni defects in otherwise pristine surfaces of
91 FeS?
- 92 (2) How does substitutionally incorporated Ni distribute itself across the surfaces of
93 FeS?
- 94 (3) What influence does Ni exert on the adsorption of CO₂ onto the surfaces of FeS?

95 2. Computational details

Spin-polarized density functional theory calculations were performed using the Vienna ab-initio simulation package (VASP) [37–39] with the projector-augmented wave (PAW) method and a plane-wave cutoff of 400 eV. For the PAW potentials, the valence electronic configurations used were $4s^13d^7$ for iron and $3s^23p^4$ for sulphur.

The general gradient approximation (GGA) for the exchange-correlation (XC) functional was employed within the Perdew-Burke-Ernzerhof (PBE) parametrization [40]. Long distance dispersion corrections were included using the D3 approach of Grimme *et al* [41]. The conjugate gradient method was used for structural optimisations, with the total energy and force convergence criteria set to 10^{-5} eV and 0.01 eV/Å. The Brillouin zone was sampled using $9 \times 9 \times 7$ and $9 \times 9 \times 1$ Γ -centred Monkhorst-Pack meshes for the bulk and surfaces of FeS, respectively [42]. The nickel-doped surfaces as well as the CO₂ adsorption and dissociation calculations were sampled on a $5 \times 5 \times 1$ Γ -centred mesh of k-points.

The extent of charge distributions was studied using the Bader scheme as implemented in the Henkelman code [43–45]. Graphical drawings were produced using VESTA [46]. The d-band centre was obtained using the VASPKIT program [47]. The transition states and activation barriers were determined with the climbing-image nudged elastic band (cNEB) method [48–50].

Defect calculations

The formation energy of a neutral defect E^f is defined as [51]:

$$E^f(D) = E_{tot}(D) - E_{tot}(H) - \sum_i n_i \mu_i,$$

where $E_{tot}(D)$ and $E_{tot}(H)$ are the respective total energies of the system with and without the defect, respectively. The value of n_i represents the number of atoms of element i that are added ($n_i > 0$) or removed ($n_i < 0$) from the supercell to form the defect, and μ_i is the chemical potential of element i , which can be written as $\mu_i = \mu_i^{elem} + \Delta \mu_i$, where μ_i^{elem} is the chemical potential of element i in its standard phase, with reference to the total energy of the elementary phases at zero Kelvin (i.e., Fe(s) and S₈(g)).

The allowed values of $\Delta \mu_i$ are determined from a set of thermodynamic limits. The upper limit is defined through $\Delta \mu_i$ where element i precipitates to its standard phase, which in this case reads metallic iron and molecular sulphur in the gas phase. Further, to avoid the formation of secondary solids, the chemical potentials must be bound by

$$\Delta \mu_{Fe} + 2 \Delta \mu_S \leq \Delta H_f(FeS_2), 3 \Delta \mu_{Fe} + 4 \Delta \mu_S \leq \Delta H_f(Fe_3S_4), \\ 7 \Delta \mu_{Fe} + 8 \Delta \mu_S \leq \Delta H_f(Fe_7S_8),$$

with ΔH_f being the standard enthalpy of formation at zero Kelvin. The total energies of the phases competing with FeS were calculated using their respective unit cells. FeS₂ and Fe₃S₄ were modelled with a simple cubic cell, while Fe₇S₈ was modelled using the low temperature ferrimagnetic monoclinic phase.

Finally, to maintain the thermodynamic equilibrium with FeS, the chemical potentials are additionally constrained by the condition:

$$\Delta \mu_{Fe} + \Delta \mu_S \leq \Delta H_f(FeS).$$

The outlined chemical potential analysis yields a Fe-rich/S-poor environment with $\Delta \mu_{Fe} = 0$, $\Delta \mu_S = -1.023$ and Fe-poor/S-rich environment with $\Delta \mu_{Fe} = -0.503$, $\Delta \mu_S = -0.519$.

Upon doping, the solubility of the Ni species is limited by the formation of the secondary phase, FeNi₂S₄ (the mineral violarite)

$$\Delta \mu_{Fe} + 2 \Delta \mu_{Ni} + 4 \Delta \mu_S \leq \Delta H_f(FeNi_2S_4),$$

where $\Delta \mu_{Ni}$ can be calculated to be 0.738 under Fe-rich/S-poor conditions and -0.016 under Fe-poor/S-rich conditions, with only the latter value being physically relevant.

Surface calculations

The METADISE code [52] was employed to create the three dominant low Miller index surfaces of FeS, namely (001), (011), and (111). The surfaces were modelled as a slab of material with periodic boundary conditions in the plane direction and a vacuum layer in the direction orthogonal to the surface. A vacuum region of at least 15 Å was tested to be sufficient to avoid interactions between the periodic slabs.

To characterize the surfaces, the surface energy (γ) as a measure of the thermodynamic stability has been calculated through the following formalism [53]:

$$\gamma_{\text{unrelaxed}} = \frac{E_{\text{unrelaxed-slab}}^{\text{DFT}} - n \times E_{\text{bulk}}^{\text{DFT}}}{2 A_{\text{slab}}}, \gamma_{\text{relaxed}} = \frac{E_{\text{relaxed-slab}}^{\text{DFT}} - n \times E_{\text{bulk}}^{\text{DFT}}}{A_{\text{slab}}} - \gamma_{\text{unrelaxed}},$$

where $\gamma_{\text{unrelaxed}}$ and γ_{relaxed} are the surface energies before and after relaxation, $E_{\text{unrelaxed-slab}}^{\text{DFT}}$, $E_{\text{relaxed-slab}}^{\text{DFT}}$, and $E_{\text{bulk}}^{\text{DFT}}$ are the DFT energies of the unrelaxed and relaxed slab and bulk, respectively, A_{slab} is the surface area, and n is the ratio between the number of atoms in the slab and in the bulk.

The adsorption energy of CO₂ (E_{ads}) was calculated from the fully atomically relaxed geometries. The total energy of the slab with the adsorbate ($E_{\text{slab+adsorbate}}$), the energy of the adsorbate ($E_{\text{adsorbate}}$), and pristine slab energy (E_{slab}) are related via the following expression:

$$E_{\text{ads}} = E_{\text{slab+adsorbate}} - (E_{\text{slab}} + E_{\text{adsorbate}}),$$

where negative adsorption energy values indicate energetically favourable exothermic processes, while positive energies correspond to endothermic processes.

3. Results and discussion

Bulk and pristine FeS surfaces

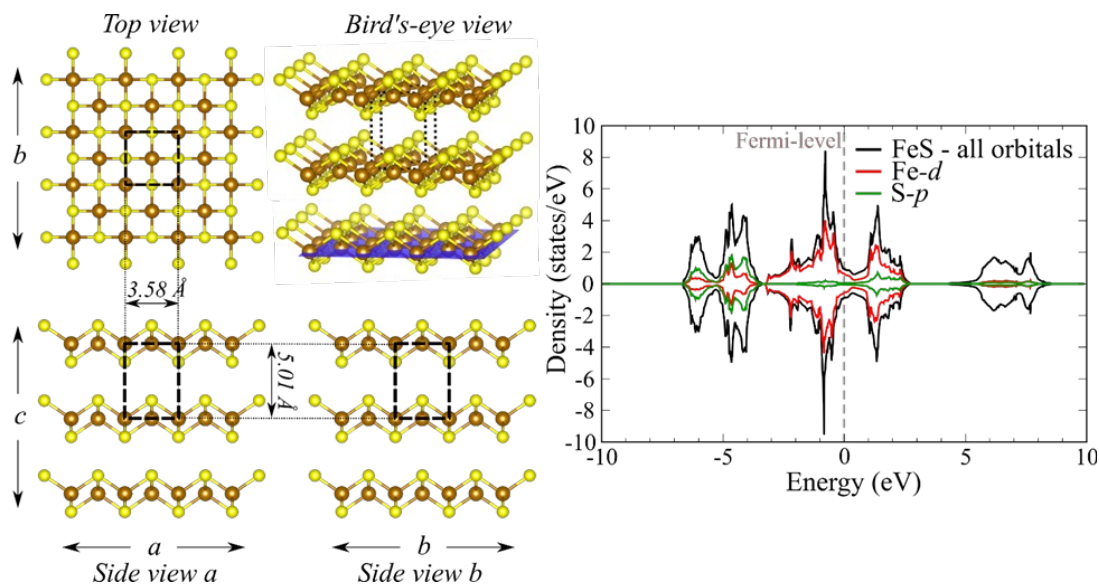


Figure 1. Crystal structure of bulk FeS mackinawite shown on the left. The unit cell is indicated with black striped lines, while sulphur and iron atoms are coloured yellow and brown, respectively. The total electronic densities of states, together with the orbital projected ones are shown on the right.

Bulk mackinawite forms in a tetragonal crystal structure (space group $P4/nmm$, number 129), with the conventional cell containing two iron and two sulphur atoms (structure shown in Figure 1). The calculated lattice parameters ($a = 3.581 \text{ \AA}$ and $c = 5.011 \text{ \AA}$) reproduce within a few percent the experimentally observed values [54], similar to the findings in earlier studies [24].

The calculated relaxed surface energies of the three dominant surfaces of FeS are listed in Table 1. The obtained values match very well with the trends observed in previous works, with the differences being attributed to the use of a disparate exchange-correlation functional and correction for long-range interactions. The (001)-S surface was

found to be the dominant surface of FeS, as the creation of the surface breaks effectively only the weak Van der Waals interlayer interaction and as such does not alter the coordination number of any Fe or S atoms. This observed high stability of the (001)-S surface is also in line with earlier experimental findings [54]. Despite the high energy required to form certain surfaces (particularly the (001)-Fe termination), all surfaces were tested in subsequent defect calculations.

Table 1. Calculated relaxed surface energies of three low Miller index surfaces of FeS.

Surface	Termination	Relaxed surface energy, γ_{relaxed} (J/m ²)	Other works [24]	theoretical
(001)	S	0.23	0.19	
	Fe	3.55	N/A	
(011)	S	1.14	1.47	
	Fe	1.15	0.95	
(111)	S	1.27	1.51	
	Fe	1.66	1.69	

Ni-doped FeS surfaces

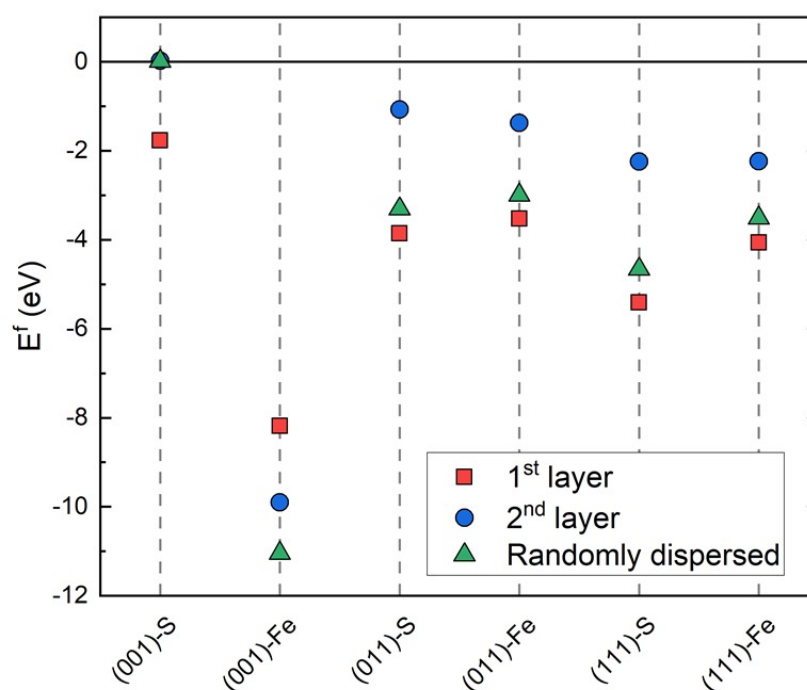


Figure 2. Calculated defect formation energies of selected Ni doped FeS surfaces.

To model FeS surfaces doped with Ni in the desired ratio of 1:5 (1 Ni atom for every 5 Fe atoms, which is accessible within the experimental regime [34,55]), 2x2 supercells were created from the previously relaxed systems, with several Fe atoms substituted by Ni atoms. Three possible arrangements (scenarios) were modelled: Ni atoms substituting the first layer of Fe atoms, Ni atoms replacing the second layer of Fe atoms in the slab, and Ni atoms found randomly dispersed throughout the simulation cell. [A random number generator was used to obtain the dispersed distribution of Ni atoms throughout the surfaces, with the final geometries available in the supplementary file.](#)

197 The calculated formation energies of the Ni-doped FeS surface are shown in Figure
198 2. The first observation is that all defects have negative formation energies (with only
199 slightly positive values in the case of the 001-S terminated surface). This indicates
200 spontaneous substitution of Fe atoms with Ni ones, i.e., no energy investment is
201 necessary to form the defects. This indicates that difficulties may be met in controlling
202 the doping process when incorporating Ni into the FeS in the desired Ni:Fe ratio.
203 Despite such seemingly unphysical results, they agree well with previous experimental
204 studies which demonstrated a high uptake of Ni²⁺ ions by mackinawite [32,34,55].
205 Likewise, earlier theoretical studies noted that metal substitution of Fe (by Co, Ni, and
206 Cu) is thermodynamically more favoured over intercalation in bulk mackinawite
207 FeS [33].

208 A trend amongst the (011) and (111) surfaces is noted, where the Ni dopants
209 substituting Fe in the first layer and the ones randomly dispersed through the surface
210 are energetically always preferred over the counterpart occurring in the first subsurface
211 layer. Defects occupying the sub-surface layer interact strongly and induce considerable
212 lattice relaxation in both directions along the z-axis (perpendicular to the surface),
213 whereas defects in the first layer can more easily extend into the space above the surface.
214 The competitive interplay between the dopants in the first layer and randomly dispersed
215 ones explains the experimentally noted slow Ni uptake process in FeS which indicated a
216 combination of Ni intercalated between S-S layers and diffusion-controlled lattice
217 penetration and structural substitution [34].

218 The optimized structures of the doped surfaces are shown in Figure 3. The (001)-Fe
219 terminated surface undergoes the most significant structural reconfiguration (in all
220 considered scenarios) as a result of the surface accommodating the dopant atoms. The Fe
221 and Ni atoms undergo relaxation into the surface, bridging the underlying tetrahedral
222 sheets and forming a regular S-terminated configuration, in the case of the (001)-Fe
223 surface doped randomly and with dopants the second-layer, which reflects the high
224 surface energy outlined earlier; the (001)-Fe surface requires a substantial energetic
225 investment to form and reorganizes promptly upon small perturbations. The remaining
226 surfaces show negligible relaxation when doped with Ni, predominantly as a result of
227 the elongated Ni-S bond lengths (compared to the initial Fe-S bonds) arising from the
228 increased Coulomb repulsion between electrons.

229 The obtained results are in good agreement and complement existing experimental
230 findings. For example, Wilkin *et al* [34] measured a slightly elongated Ni-S bond distance
231 of (2.28 ± 0.01) Å in Ni-doped mackinawite, compared to a Fe-S distance of 2.26 Å in Ni-
232 free mackinawite. In the same study, a coordination number of (4.04 ± 0.30) was derived
233 for mackinawite with composition Fe_{0.58}Ni_{0.42}S, close to the 4-fold Fe coordination in
234 pristine FeS. Despite these results obtained for a bulk sample of synthetic FeS and an
235 increased Ni-content, similar behaviour of elongated Ni-S bond distances and preserved
236 4-fold coordination was observed for the Ni-doped surfaces of mackinawite FeS
237 considered in this study.

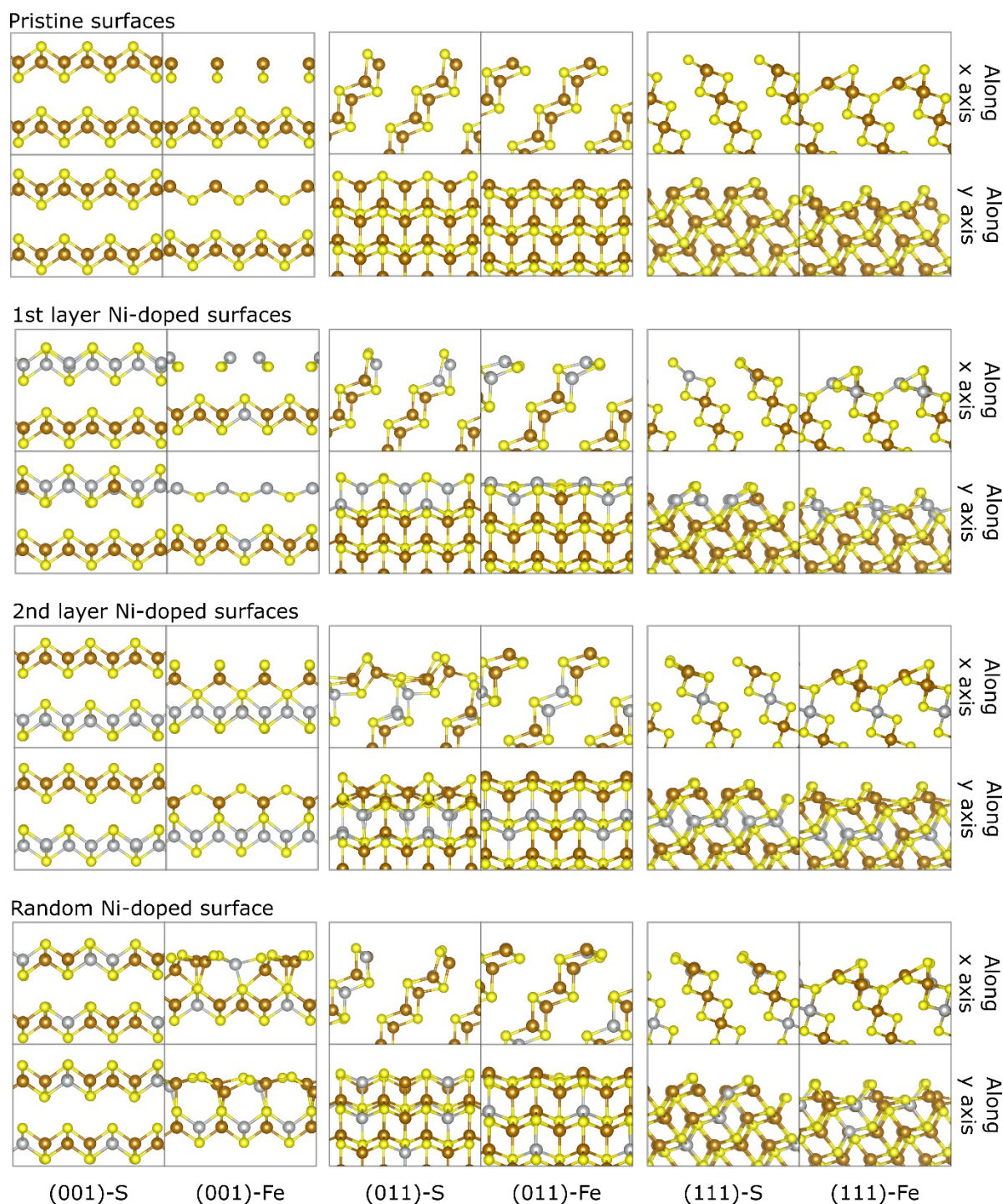
238
239

Figure 3. Optimized structures of the relaxed pristine as well as Ni doped FeS surfaces of choice. Brown, yellow, and grey spheres represent iron, sulphur, and nickel atoms, respectively.

240

Adsorption and activation of CO₂ on pristine vs. Ni-doped FeS surfaces

241
242
243

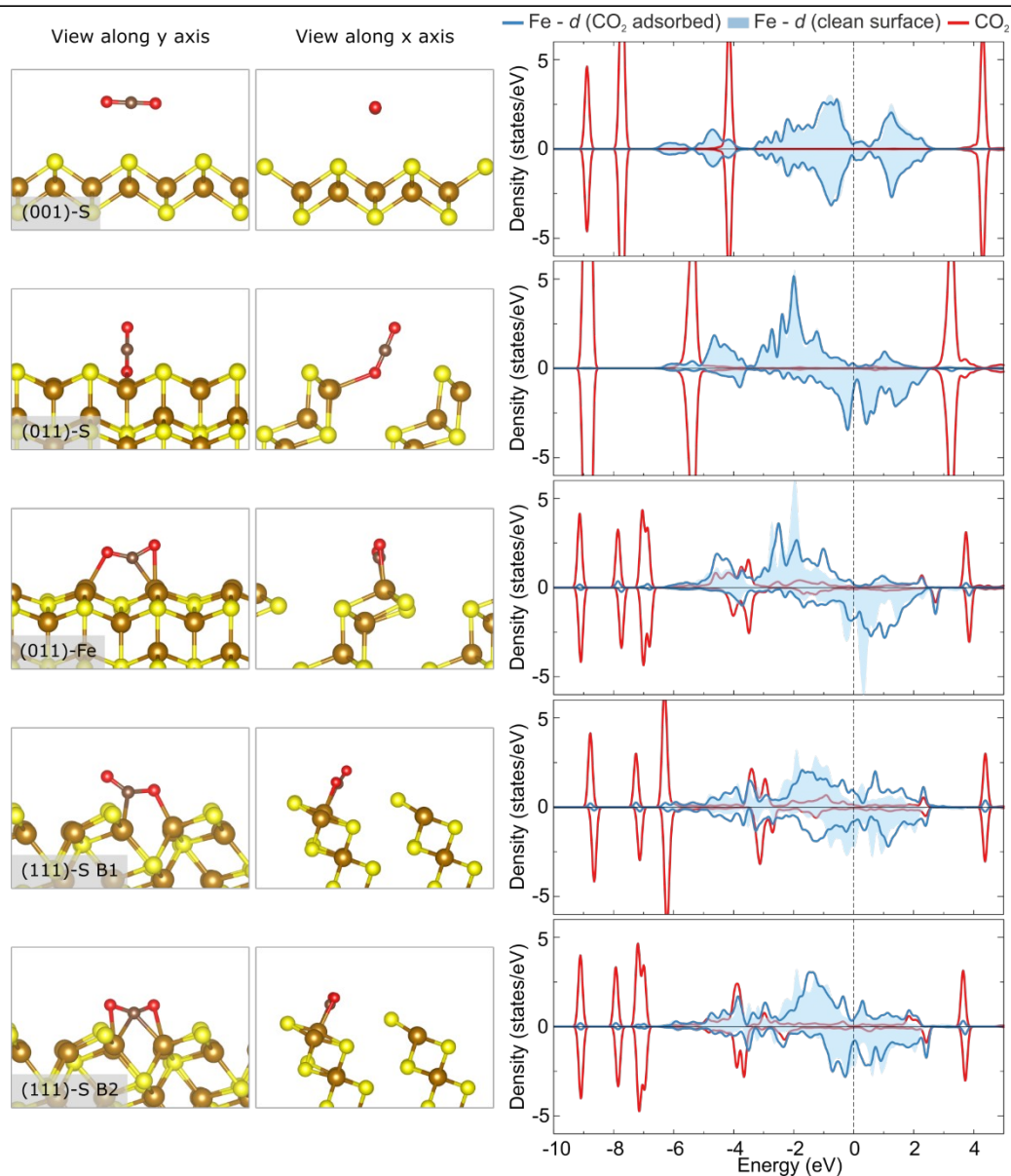
Table 2. Calculated adsorption energy (E_{ads}), CO₂ inner angle ($\angle(\text{O-C-O})$), and O-C bond stretching (O1-C/O2-C) of a single CO₂ molecule adsorbed on three pristine low Miller index surfaces of FeS mackinawite. The B1 and B2 adsorption position nomenclature were taken from the work of Dzade et al [24].

Pristine surface	Adsorption position	E_{ads} (eV)	$\angle(\text{O-C-O})$ ($^{\circ}$)	O1-C/O2-C stretching (%)
(001)-S	Top Fe	-0.01	180.0	0.0/0.0
	Top S	-0.01	180.0	0.0/0.0
(001)-Fe	Top Fe	No stable config/ surface reconfiguration observed		
	Top S	No stable config/ surface reconfiguration observed		
(011)-S	Top Fe	-0.23	178.6	0.7/-0.7
	Top S	0.01	180.0	0.0/0.0
(011)-Fe	Top Fe	-0.54	138.2	6.6/5.9
	Top S	-0.17	178.9	-0.5/0.6
(111)-S	Top Fe	0.33	133.0	9.6/2.9
	Top S	No stable config		
	B1	-0.99	133.4	5.6/5.6
	B2	-1.29	139.2	3.1/5.6
(111)-Fe	Top Fe	No stable config/ surface reconfiguration observed		
	Top S	No stable config/ surface reconfiguration observed		

The adsorption of CO_2 was first performed on the pristine surfaces of FeS mackinawite, to define a reference point for comparison with the Ni-doped surfaces. The single CO_2 molecule introduced on the (001)-S terminated surface moved away perpendicular from the surface during the atomic relaxation and energy minimization process, regardless of the initial placement of the molecule. The distance between the surface and the adsorbate was found to be larger than 5 Å, confirming the non-existing adsorption noted by a vanishing adsorption energy value (Table 2).

Adsorption of carbon dioxide on top of the (001)-Fe surface was tested for completeness of the results, yet no stable configuration was determined. The surface also underwent strong reorganization turning itself effectively into an S-terminated plane, confirming the difficulty of stabilizing and achieving control over this particular surface.

In contrast to the (001) surface, CO_2 is found to physisorb onto the sulphur terminated (011) and chemisorb onto the iron-terminated (011) surface of $-\text{FeS}$ mackinawite, in both cases at an exposed Fe site (Table 2). In the case of (011)-S, CO_2 binds solely through an O atom interacting with the exposed Fe site, leading to negligible changes in the bond length and angles of the adsorbate. The adsorption configuration of CO_2 at the (011)-Fe surface matches well the bent configuration labelled as B(III) in the work of Dzade *et al* [24], where the molecule binds actively through one O and a C atom to two surface Fe atoms. The molecule also undergoes significant bending, and the O-C bond is stretched considerably, indicating possible activation (depicted in Figure 4). On the (111) surface, carbon dioxide was found to adsorb strongly in two configurations on the S-terminated surface, but there was no similar counterpart observed on the Fe-terminated surface.



267
268

Figure 4. Optimized structures of the CO₂ molecule adsorbed on the pristine surfaces of FeS (left) together with the accompanying electronic densities of the state (right).

269
270
271
272
273
274

For the subsequent study of CO₂ adsorption on the Ni-doped surfaces, the pristine surfaces with the strongest adsorption tendency were chosen, namely (001)-S, (011)-Fe, and (111)-S. Ni-doping was considered as the case of randomly dispersed substitutional atoms throughout the surface.

As with the undoped surfaces, the CO₂ molecule does not adsorb on the Ni-doped (001)-S surface, regardless of the initial placement (complete results listed in Table 3).

Table 3. Calculated adsorption energy (E_{ads}), CO_2 inner angle ($\angle(\text{O-C-O})$), and O-C bond stretching (O1-C/O2-C) of a single CO_2 molecule adsorbed on various Ni-doped surfaces of FeS mackinawite. The B1 and B2 adsorption position nomenclature were taken from the work of Dzade et al [24]. In the “-alt” notation, the position of the most prominent Fe and Ni atoms was swapped, to test for eventual differences.

Ni-doped surface	Adsorption position	E_{ads} (eV)	$\angle(\text{O-C-O})$ ($^\circ$)	O1-C/O2-C stretching (%)
(001)-S	Top Fe	0.06	180.0	0.0/0.0
	Top S-1	0.07	180.0	0.0/0.0
	Top S-2	0.08	180.0	0.0/0.0
	Top Ni	0.06	180.0	0.0/0.0
(011)-Fe	Top Fe	-0.14	148.1	6.2/1.9
	Top S	-0.09	179.2	0.1/-0.1
(111)-S	B1	0.14	139.5	3.1/6.6
	B1 – alt	-0.11	178.9	-0.6/0.6
	B2	-0.53	143.9	5.7/1.8
	B2 – alt	-0.78	178.9	-0.6/0.6

The adsorption of CO_2 on top of the Ni-doped (011) and (111) surfaces is weakened, compared to the undoped surface. Starting from the bridged position of CO_2 on the pristine surface, the molecule desorbs from the site where Ni atom substituted Fe (surface structure depicted in Figure 5). The molecule on top of the (011)-Fe surface rotates away from the Ni atom and stays bound on top of the most prominent Fe atom in an activated state, while CO_2 on top of the (111) surface deactivates into a linear conformation, binding weakly to the surface through one of its O atoms.

The changes in the binding mechanism are further illustrated through the calculated electronic densities of state shown in Figure 5. The electronic states of CO_2 adsorbed on top of the (001) surface shown distinct peaks with negligible changes between the pristine and Ni-doped scenario. In contrast, in the case of the (011) and (111) surfaces, the broadened states overlapping with prominent surface Fe atoms (present around -3 eV) transform into distinct states when Ni is present in the surface.

To quantify the effect of Ni-doping onto the surfaces of FeS, the centre of the surface d -band was computed, as this property has been linked successfully to understanding and predicting the catalytic activity of transition metal surfaces [56]. Upon Ni-doping, the centre of the d -band experiences a downwards shift (average value) of about $\Delta = 0.25$ eV, 0.26 eV, and 0.28 eV in the case of the (001)-S, (011)-Fe, and (111)-S surfaces, respectively. Such a downward shift lowers the possibility to form a large number of empty anti-bonding states, leading to reduced binding energies of the adsorbed CO_2 molecule. The reduced number of empty states present in the Ni-doped surface is not necessarily a surprise, considering the increased number of paired electrons in the d -states of Ni, compared to the Fe atom, thereby exerting stronger Coulomb repulsion towards the adsorbate.

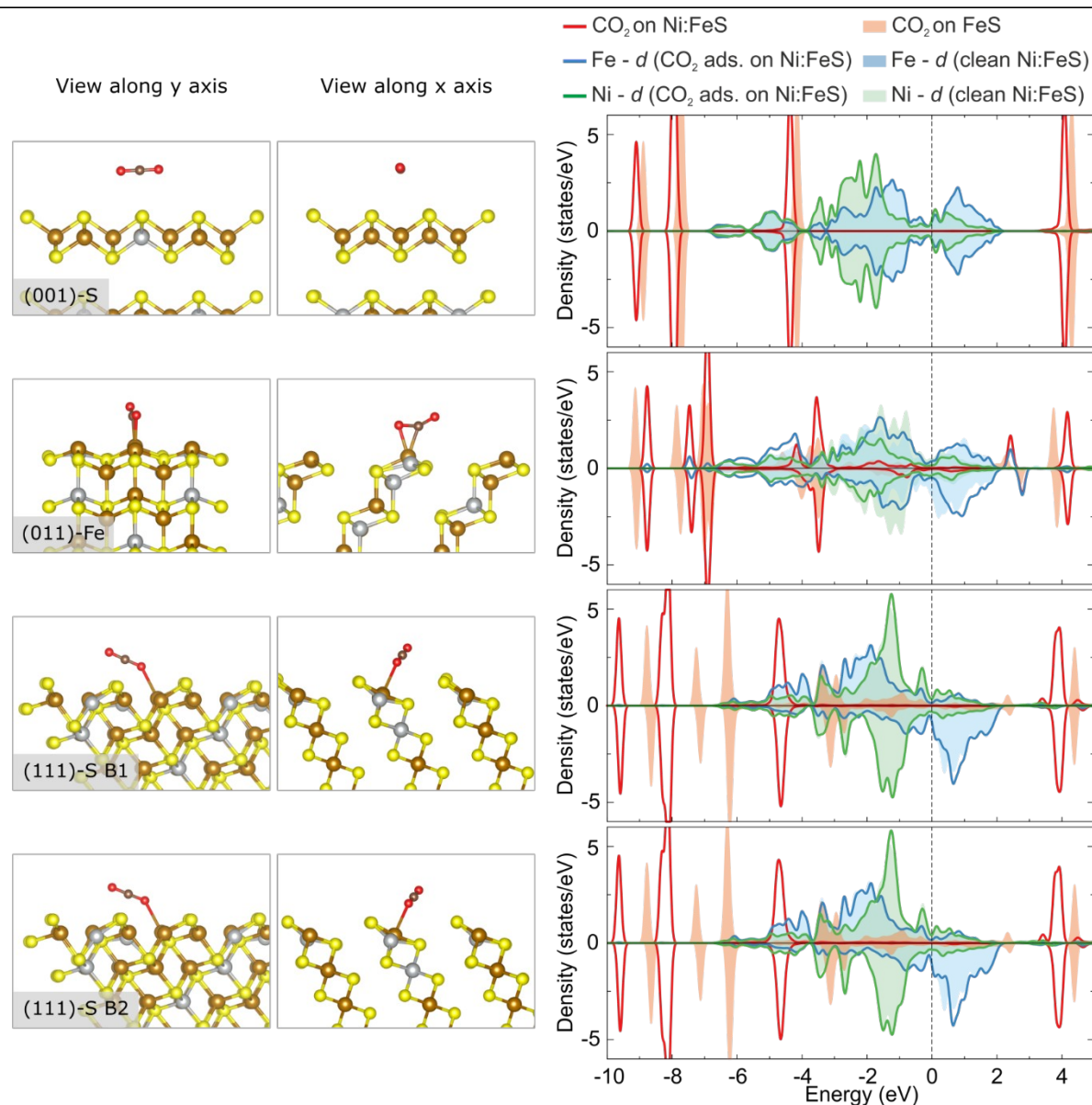


Figure 5. Crystal structure of the CO₂ molecule adsorbed on the Ni-doped surfaces of FeS (left) together with the accompanying electronic densities of the state (right).

CO₂ dissociation on Ni-doped FeS surfaces

So far, the influence of Ni on the strength of CO₂ adsorption on the surface of FeS was considered. There is still the question whether Ni dopants can also dictate the reactivity of the system with respect to CO₂ dissociation into surface-bound CO and O species. To analyse this process, the (011)-Fe and (111)-S terminated surfaces were considered for subsequent transition state calculations to obtain reaction energies and activation barriers.

The calculated minimum energy profiles for CO₂ dissociation from the chosen starting structures on the (011)-Fe and (111)-S surface are shown in Figure 6. The calculated reaction energy at the (011)-Fe surface indicates that the dissociation is an endothermic process with a cost of +0.85 eV. In the final configuration the dissociated O species binds to a surface S ($d(\text{O-S}) = 1.49 \text{ \AA}$) and the remaining CO binds through the C atom to the first prominent Fe atom ($d(\text{C-Fe}) = 1.73 \text{ \AA}$). Such behaviour is similar to the one that Dzade *et al* [24] observed for CO₂ dissociation at a pristine (011) surface. However, the activation energy of 2.39 eV is significantly increased compared to the 1.25 eV calculated for the same process occurring at an undoped surface.

The situation at the (111)-S surface is quite different. Splitting CO₂ into CO+O starting from the B1 position outlined earlier proceeds as an exothermic reaction releasing 0.32 eV in energy, with a final configuration where O bridges one Fe and one Ni atom and CO attaches to an adjacent Fe atom but avoiding the most prominent Ni atom. The activation energy is calculated at 1.45 eV, which is a value that is doubled compared to the 0.72 eV for CO₂ dissociation on top a undoped (111)-S surface.

In contrast, splitting of CO₂ from the initial B2 position on the (111)-S surface proceeds towards a state where the CO moiety weakly interacts atop a Ni atom and the remaining O binds to a prominent Fe atom. The C-Ni bond length is measured at 1.84 Å, which contrasts with the C-Fe bond length of 1.76 Å, indicating a weaker interaction when compared to the CO₂ split from the B1 configuration. The calculated reaction energy reveals that this process is highly endothermic, requiring +2.52 eV to materialize, further confirming the reduced impact Ni plays for the catalytic properties of mackinawite. The activation energy is calculated at almost 3 eV, rendering this ~~dissociation~~ dissociation scenario highly unfavourable.

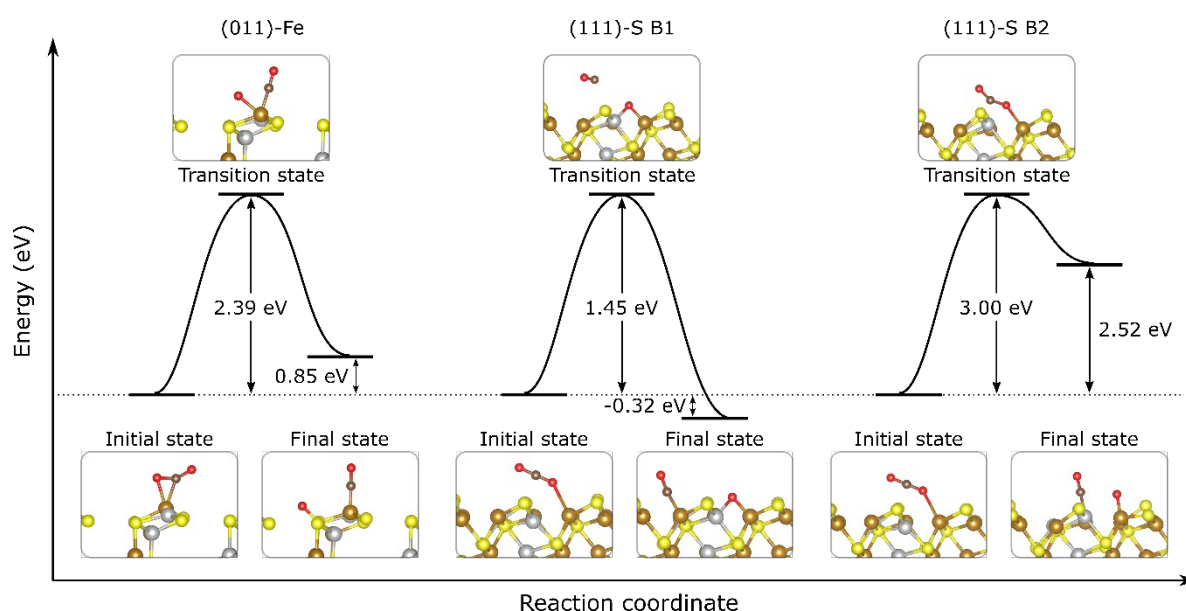


Figure 6. Calculated potential energy profile for CO₂ dissociation on Ni-doped FeS mackinawite surfaces.

Conclusion

A computational study of the effect of substitutional Ni doping on the most prominent surfaces of FeS mackinawite was undertaken using DFT-D3 calculations. Three different doping patterns were studied for Ni incorporated at the Fe site as well as the possible effect of the dopant on the adsorption and activation of CO₂. Following the results presented above, several significant conclusions can be drawn:

- Ni is readily incorporated substitutionally at the Fe site into the FeS matrix, where low formation energies indicate that it may be difficult to control the dopant concentration.
- FeS surfaces doped with Ni exhibit weaker binding as well as deactivation of adsorbed CO₂ molecules, when compared to the same process on undoped mackinawite surfaces.
- The (average) position of the *d*-band centre of the Ni doped surfaces of FeS mackinawite is found at a consistently lower position than it is at the pristine surfaces. This is linked to the electronic configuration of Ni atoms which is closer to a closed-shell system than that of the open *d*-orbitals of Fe atoms.

The results presented here indicate a reduced activity of Ni-doped surfaces of FeS mackinawite towards the possible activation and dissociation of CO₂. However, care should be taken when interpreting these results, as certain limitations apply. The system

under scrutiny was subjected neither to varying temperatures and pressures, nor has it included competitive adsorbates such as water or oxygen, which are known to have a strong effect on the stability of mackinawite [28,32]. For example, in a recent work, Hudson *et al* [57] reported reduction of CO₂ with H₂ to formate (HCOO⁻) across Fe(Ni)S precipitates. Direct comparison with such works is very difficult, owing to the vast number of variables not available in the presented study, such as pH and redox gradients. More importantly, Dzade *et al* [58] unravelled the role that sulphur vacancies play in promoting CO₂ and H₂ adsorption on the FeS(001) basal plane. It would be of considerable interest to include sulphur and iron vacancies together with Ni dopants in a follow up work to probe their synergic effect onto the adsorption properties of FeS surfaces. Nevertheless, this study was able to probe the isolated effect of pure Ni-doping onto the catalytic properties of mackinawite and unravel some of the roles that Ni incorporation could play in the diverse group of iron sulphide solids.

Acknowledgments: A.Z. and N.H.d.L acknowledge the NWO ECHO grant (712.018.005) for funding. E.C. acknowledges NWO and the Dutch Origins Center for funding. Part of the local compute cluster and the research work of M.W. is part of the Industrial Partnership Programme i32 Computational Sciences for Energy Research that is carried out under an agreement between Shell and the Netherlands Organisation for Scientific Research (NWO). This project has received funding from the European Research Council (ERC) under the European Union's Horizon 2020 research and innovation programme (grant agreement No 819588). This work was carried out on the Dutch national e-infrastructure with the support of SURF Cooperative.

References

- [1] A. D. Handoko, F. Wei, Jenndy, B. S. Yeo, and Z. W. Seh, *Nat. Catal.* **1**, 922 (2018).
- [2] M. Wansleben, J. Vinson, A. Wählisch, K. Bzheumikhova, P. Hönicke, B. Beckhoff, and Y. Kayser, *J. Anal. At. Spectrom.* **35**, 2679 (2020).
- [3] X. Yang and D. Wang, *ACS Appl. Energy Mater.* **1**, 6657 (2018).
- [4] C. Graves, S. D. Ebbesen, M. Mogensen, and K. S. Lackner, *Renew. Sustain. Energy Rev.* **15**, 1 (2011).
- [5] S. Xu and E. A. Carter, *Chem. Rev.* **119**, 6631 (2019).
- [6] A. Rafiee, K. Rajab Khalilpour, D. Milani, and M. Panahi, *J. Environ. Chem. Eng.* **6**, 5771 (2018).
- [7] Z. W. Seh, J. Kibsgaard, C. F. Dickens, I. Chorkendorff, J. K. Nørskov, and T. F. Jaramillo, *Science (80-.)*. **355**, eaad4998 (2017).
- [8] D. J. Vaughan, U. Becker, and K. Wright, *Int. J. Miner. Process.* **51**, 1 (1997).
- [9] D. J. Vaughan, *Rev. Mineral. Geochemistry* **61**, 1 (2006).
- [10] D. S. Inosov, *Adv. Phys.* **67**, 149 (2018).
- [11] D. Rickard and G. W. Luther, *Chem. Rev.* **107**, 514 (2007).
- [12] C. Huber, *Science (80-.)*. **281**, 670 (1998).
- [13] E. Drobner, H. Huber, G. Wächtershäuser, D. Rose, and K. O. Stetter, *Nature* **346**, 742 (1990).
- [14] M. J. Russell, R. M. Daniel, A. J. Hall, and J. A. Sherringham, *J. Mol. Evol.* **39**, 231 (1994).
- [15] A. Roldan, N. Hollingsworth, A. Roffey, H. U. Islam, J. B. M. Goodall, C. R. A. Catlow, J. A. Darr, W. Bras, G. Sankar, K. B. Holt, G. Hogarth, and N. H. De Leeuw, *Chem. Commun.* **51**, 7501 (2015).
- [16] B. Herschy, A. Whicher, E. Camprubi, C. Watson, L. Dartnell, J. Ward, J. R. G. Evans, and N. Lane, *J. Mol. Evol.* **79**, 213 (2014).
- [17] U. Terranova, C. Mitchell, M. Sankar, D. Morgan, and N. H. de Leeuw, *J. Phys. Chem. C* **122**, 12810 (2018).
- [18] Y. Hu, G. Wu, R. Li, L. Xiao, and X. Zhan, *Water Res.* **179**, 115914 (2020).
- [19] Q. Li, Y. Zhang, Y. Liao, J. Huang, Z. Dang, and C. Guo, *J. Colloid Interface Sci.* **572**, 236 (2020).
- [20] C. J. Vessey and M. B. J. Lindsay, *Environ. Sci. Technol.* **54**, 4006 (2020).
- [21] G. D. Cody, N. Z. Boctor, J. A. Brandes, T. R. Filley, R. M. Hazen, and H. S. Yoder, *Geochim. Cosmochim. Acta* **68**, 2185 (2004).
- [22] N. Y. Dzade, A. Roldan, and N. H. de Leeuw, *Phys. Chem. Chem. Phys.* **16**, 15444 (2014).
- [23] N. Y. Dzade, A. Roldan, and N. H. de Leeuw, *J. Chem. Phys.* **139**, 124708 (2013).
- [24] N. Y. Dzade, A. Roldan, and N. H. De Leeuw, *J. Chem. Phys.* **143**, (2015).
- [25] N. Y. Dzade, A. Roldan, and N. H. De Leeuw, *Environ. Sci. Technol.* **51**, 3461 (2017).
- [26] N. Y. Dzade, A. Roldan, and N. H. de Leeuw, *Phys. Chem. Chem. Phys.* **18**, 32007 (2016).
- [27] N. Y. Dzade, A. Roldan, and N. H. De Leeuw, *J. Chem. Phys.* **144**, (2016).
- [28] N. Y. Dzade, A. Roldan, and N. H. De Leeuw, *J. Phys. Chem. C* **120**, 21441 (2016).
- [29] M. Kolos, D. Tunega, and F. Karlický, *Phys. Chem. Chem. Phys.* **22**, 23258 (2020).
- [30] N. E. R. Ofili, A. Thetford, and N. Kaltsoyannis, *Environ. Sci. Technol.* **54**, 6792 (2020).
- [31] Q. Hu, C. Wang, Y. Geng, X. Zhang, J. Mei, and S. Yang, *J. Colloid Interface Sci.* **582**, 581 (2021).
- [32] J. W. Morse and T. Arakaki, *Geochim. Cosmochim. Acta* **57**, 3635 (1993).

- 413 [33] K. D. Kwon, K. Refson, and G. Sposito, *Am. Mineral.* **100**, 1509 (2015).
- 414 [34] R. T. Wilkin and D. G. Beak, *Chem. Geol.* **462**, 15 (2017).
- 415 [35] M. Ikogou, G. Ona-Nguema, F. Juillot, P. Le Pape, N. Menguy, N. Richeux, J. M. Guigner, V. Noël, J. Brest, B. Baptiste, and G.
416 Morin, *Appl. Geochemistry* **80**, 143 (2017).
- 417 [36] E. D. Swanner, S. M. Webb, and A. Kappler, *Am. Mineral.* **104**, 917 (2019).
- 418 [37] G. Kresse and D. Joubert, *Phys. Rev. B* **59**, 1758 (1999).
- 419 [38] G. Kresse and J. Furthmüller, *Phys. Rev. B* **54**, 11169 (1996).
- 420 [39] G. Kresse and J. Furthmüller, *Comput. Mater. Sci.* **6**, 15 (1996).
- 421 [40] J. P. Perdew, K. Burke, and M. Ernzerhof, *Phys. Rev. Lett.* **77**, 3865 (1996).
- 422 [41] S. Grimme, J. Antony, S. Ehrlich, and H. Krieg, *J. Chem. Phys.* **132**, 154104 (2010).
- 423 [42] H. J. Monkhorst and J. D. Pack, *Phys. Rev. B* **13**, 5188 (1976).
- 424 [43] M. Yu and D. R. Trinkle, *J. Chem. Phys.* **134**, 064111 (2011).
- 425 [44] W. Tang, E. Sanville, and G. Henkelman, *J. Phys. Condens. Matter* **21**, 084204 (2009).
- 426 [45] E. Sanville, S. D. Kenny, R. Smith, and G. Henkelman, *J. Comput. Chem.* **28**, 899 (2007).
- 427 [46] K. Momma and F. Izumi, *J. Appl. Crystallogr.* **44**, 1272 (2011).
- 428 [47] V. Wang, N. Xu, J. C. Liu, G. Tang, and W.-T. Geng, **1** (2019).
- 429 [48] D. Sheppard, R. Terrell, and G. Henkelman, *J. Chem. Phys.* **128**, 134106 (2008).
- 430 [49] G. Henkelman and H. Jónsson, *J. Chem. Phys.* **113**, 9978 (2000).
- 431 [50] G. Henkelman, B. P. Uberuaga, and H. Jónsson, *J. Chem. Phys.* **113**, 9901 (2000).
- 432 [51] C. Freysoldt, B. Grabowski, T. Hickel, J. Neugebauer, G. Kresse, A. Janotti, and C. G. Van De Walle, *Rev. Mod. Phys.* **86**, 253
433 (2014).
- 434 [52] G. W. Watson, E. T. Kelsey, N. H. de Leeuw, D. J. Harris, and S. C. Parker, *J. Chem. Soc. Faraday Trans.* **92**, 433 (1996).
- 435 [53] B. Farkaš, D. Santos-Carballal, A. Cadi-Essadek, and N. H. de Leeuw, *Materialia* **7**, 100381 (2019).
- 436 [54] M. Wolthers, S. J. Van der Gaast, and D. Rickard, *Am. Mineral.* **88**, 2007 (2003).
- 437 [55] M. Mansor, C. Winkler, M. F. Hochella, and J. Xu, *Front. Earth Sci.* **7**, 151 (2019).
- 438 [56] B. Hammer and J. K. Nørskov, *Adv. Catal.* **45**, 71 (2000).
- 439 [57] R. Hudson, R. de Graaf, M. Strandoo Rodin, A. Ohno, N. Lane, S. E. McGlynn, Y. M. A. Yamada, R. Nakamura, L. M. Barge,
440 D. Braun, and V. Sojo, *Proc. Natl. Acad. Sci.* **117**, 22873 (2020).
- 441 [58] N. Y. Dzade and N. H. de Leeuw, *Catalysts* **11**, 127 (2021).

442

443